BIOCHEMISTRY
including biophysical chemistry & molecular biology

Article

pubs.acs.org/biochemistry

Interaction of Human Synovial Phospholipase A2 with Mixed Lipid Bilayers: A Coarse-Grain and All-Atom Molecular Dynamics Simulation Study

Shan-Shan Qin,[†] Yang-Xin Yu,[‡] Qi-Kai Li,[§] and Zhi-Wu Yu*[,†]

[†]Key Laboratory of Bioorganic Phosphorous Chemistry and Chemical Biology (Ministry of Education), Department of Chemistry, Tsinghua University, Beijing 100084, P. R. China

[‡]Laboratory of Chemical Engineering Thermodynamics, Department of Chemical Engineering, Tsinghua University, Beijing 100084, P. R. China

[§]Department of Mechanical Engineering, Tsinghua University, Beijing 100084, P. R. China

Supporting Information

ABSTRACT: Human secreted phospholipase A2s have been shown to promote inflammation in mammals by catalyzing the first step of the arachidonic acid pathway by breaking down phospholipids, producing fatty acids, including arachidonic acid. They bind to the membrane water interface to access their phospholipid substrates from the membrane. Their binding modes on membrane surfaces are regulated by diverse factors, including membrane charge, fluidity, and heterogeneity. The influence of these factors on the binding modes of the enzymes is not well understood. Here we have studied several human synovial phospholipase A2 (hs-PLA2)/mixed bilayer systems through a combined coarse-grain and all-atom molecular dynamics simulation. It was found that hydrophobic residues Leu2, Val3, Ala18, Leu19, Phe23, Gly30, and Phe63 that form the edge of the entrance of the hydrophobic binding pocket in hs-PLA2 tend to penetrate into the hydrophobic area of lipid bilayers, and more than half of the total amino acid residues make contact with the lipid headgroups. Each enzyme molecule forms 19−38 hydrogen bonds with the bilayer to which it binds, most of which are with the phosphate groups. Analysis of the root-mean-square deviation (rmsd) shows that residues Val30−Thr40, Tyr66−Gln80, and Lys107−Arg118 have relatively large rmsds during all-atom molecular dynamics simulations, in accordance with the observation of an enlarged entrance region of the hydrophobic binding pocket. The amino acid sequences forming the entrance of the binding pocket prefer to interact with lipid molecules that are more fluid or negatively charged, and the opening of the binding pocket would be larger when the lipid components are more fluid.

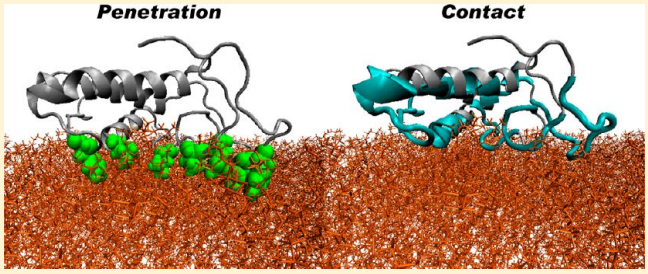

Phospholipase A2s (PLA2s) make up a family of enzymes that catalyze the hydrolysis of the *sn*-2 ester bond of glycerophospholipids. They are involved in a range of cellular processes, including the release of lipid mediators, membrane remodeling, inflammation, and transmembrane signaling. These enzymes can be roughly classified into two categories: the 14 kDa secretory PLA2 (sPLA2)[1,2] and the 80 kDa cytosolic PLA2 (cPLA2).[1,3] sPLA2s are mainly α-helical and exist on the extracellular face of cell membranes. Human secretory phospholipase A2 is commonly regarded as a regulatory factor in many physiological processes,[3,4] and altered levels of human secretory phospholipase A2 are observed in many pathological situations, including cancer,[5] respiratory allergy,[6] and apoptosis.[7] One of its hydrolysis products, arachidonic acid, is the precursor for producing eicosanoids, including leukotrienes, thromboxanes, and prostaglandins, which are categorized as mediators of inflammation.

Human synovial PLA2 (hs-PLA2) was isolated from the synovial fluid of patients with rheumatoid arthritis. It has been thoroughly investigated through structural, biophysical, and biochemical methods.[8,9] Scott et al.[10] determined the crystal structure of the calcium-bound form of a human nonpancreatic secretory phospholipase A2 that is found in high concentrations in the synovial fluid of patients with rheumatoid arthritis at physiological pH and identified a cluster of hydrophobic residues (Leu2, Val3, Leu19, Phe23, Val30, and Phe63) that are located at the edge of the entrance to the hydrophobic binding pocket where hydrolyzing reactions occur. They proposed that the catalytic cycle of group I/II/V PLA2s involves activation of a conserved water molecule in the active site by the H48/D99 pair, followed by nucleophilic attack on the *sn*-2 position of the phospholipid to form a tetrahedral reaction intermediate. Diez et al.[11] investigated the reaction capability of human phospholipase A2 with different phospholipid substrates and

Received: September 16, 2012
Revised: January 23, 2013
Published: January 24, 2013

   dx.doi.org/10.1021/bi3012687 | *Biochemistry* 2013, 52, 1477−1489

Table 1. Details of the Simulated Systems

	components		duration	
system	coarse-grained	full atomic	coarse-grained	full atomic
PLA2/DOPC	PLA2, 128 DOPC, 3000 CG water	PLA2, 128 DOPC, 6974 water, ions	2.5 μs	120 ns
			8.0 μs	160 ns
PLA2/DOPE	PLA2, 128 DOPE, 3000 CG water	PLA2, 128 DOPE, 6310 water, ions	2.5 μs	120 ns
			8.0 μs	160 ns
PLA2/SAPE/DOPC	PLA2, 51 SAPE, 77 DOPC, 3000 CG water	PLA2, 51 SAPE, 77 DOPC, 8005 water, ions	3.2 μs	120 ns
			8.0 μs	160 ns
PLA2/SAPE/DOPE	PLA2, 51 SAPE, 77 DOEC, 3000 CG water	PLA2, 51 SAPE, 77 DOPE, 6591 water, ions	3.2 μs	120 ns
			8.0 μs	160 ns
PLA2/SAPG/DOPC	PLA2, 51 SAPG, 77 DOPC, 3000 CG water	PLA2, 51 SAPG, 77 DOPC, 6755 water, ions	3.2 μs	120 ns
			8.0 μs	160 ns
PLA2/SAPG/DOPE	PLA2, 51 SAPG, 77 DOPE, 3000 CG water	PLA2, 51 SAPG, 77 DOPE, 7944 water, ions	3.2 μs	120 ns
			8.0 μs	160 ns
PLA2/SAPM/DOPC	PLA2, 51 SAPM, 77 DOPC, 3000 CG water	PLA2, 51 SAPM, 77 DOPC, 7970 water, ions	3.2 μs	120 ns
			8.0 μs	160 ns
PLA2/SAPM/DOPE	PLA2, 51 SAPM, 77 DOPE, 3000 CG water	PLA2, 51 SAPM, 77 DOPE, 7171 water, ions	3.2 μs	120 ns
			8.0 μs	160 ns

reached the conclusion that the human synovial fluid PLA2 shows a clear preference for *sn*-glycero-3-phosphoethanolamine over *sn*-glycero-3-phosphocholine. Jain et al. proved that phospholipase A2 hydrolyzes phospholipid vesicles in the scooting mode[12,13] and hopping mode[14] for anionic and zwitterionic membranes, respectively, and it hydrolyzes only the substrate molecules in the outer monolayer of the vesicles to which it is bound. Previous experimental studies proved that phospholipase A2 first needed to bind to the outer surface of the plasma membrane before hydrolyzing lipid molecules,[12] and its binding constants and reaction activities were found to be different when the membrane composition varied.[11,15,16] It is of importance, therefore, to examine the molecular mechanism of binding of phospholipase A2 to biomembranes with different compositions. Besides, the phospholipase A2−membrane complex is a good model for membrane-associated proteins binding to biomembranes when they are biologically functional. Thus, obtaining a detailed model of the interactions between the secretory phospholipase A2 and the lipid−water interface would be of great interest.

Although the atomic-resolution crystal structures of sPLA2s that have been determined to date can provide the three-dimensional atom coordinates of the enzymes, these coordinates were determined without considering the influence of cellular membranes and, therefore, provide little or no information about the configuration of the protein when they are functionally active, whereas computational methods are feasible for investigating the atomic binding mode of sPLA2 at the lipid−water interface. Atomistic molecular dynamics (MD) simulation is a widely used computational method for studying the structures of membrane proteins,[17−21] and this method has been used to investigate the conformational dynamics of sPLA2s and their interaction with lipid membranes. Zhou and Schulten once studied the desolvation of lipid molecules in a complex of the human synovial phospholipase A2 and a dilaurylphosphatidylethanolamine (DLPE) monolayer surface by means of molecular dynamics simulations, and the results showed that the desolvation of lipid molecules occurred in a tightly bound membrane−protein complex and the desolvated lipid molecules interacted mainly with hydrophobic protein residues.[22]

The shortcoming of the computational work involved in atomistic MD simulations of membrane proteins is the limit on the simulation time, usually within hundreds of nanoseconds. This time scale may not be sufficient to allow the equilibrium configuration to which a surface-active enzyme/bilayer system would relax. In a different way, the reduced accuracy of the coarse-grained (CG) model allows one to probe the structural dynamics of large systems on time scales of up to milliseconds,[23−26] which allows one to optimally locate a surface-active enzyme on a lipid bilayer. Wee et al. used the CG model to depict the depth of penetration of porcine pancreatic sPLA2 into a mixed POPG/POPC bilayer and evaluated the simulation results by comparing them with available experimental data.[27] The CG model, however, loses atomistic details of interesting configurations; thus, combining the efficiency of the CG model with the accuracy of the all-atom model would be a great idea for studying membrane protein/bilayer systems. This strategy has been employed in this work.

In this work, we first used the CG−MD simulations to obtain fully equilibrated configurations of human synovial phospholipase A2 binding to different mixed lipid bilayers. Two of the five glycerophospholipid molecules were chosen to form binary mixed bilayers: dioleoylphosphatidylcholine (DOPC), dioleoylphosphatidylethanolamine (DOPE), 1-stearoyl-2-arachidonoyl-*sn*-glycero-3-phosphatidylethanolamine (SAPE), 1-stearoyl-2-arachidonoyl-*sn*-glycero-3-phosphatidylglycerol (SAPG), and 1-stearoyl-2-arachidonoyl-*sn*-glycero-3-phosphatidylmethylene glycol (SAPM). In total, eight systems were simulated with the CG model (PLA2/DOPC, PLA2/DOPE, PLA2/SAPE/DOPC, PLA2/SAPE/DOPE, PLA2/SAPG/DOPC, PLA2/SAPG/DOPE, PLA2/SAPM/DOPC, and PLA2/SAPM/DOPE), each with a duration of 2.5−3.2 μs. Membrane-bound configurations of PLA2 were found to be similar among all simulated systems, with the enzyme positioned at the lipid−water interface and certain amino acid residues penetrating into the lipid bilayer. For longer times of CG simulation of up to 8 μs (Figures S1 and S2 of the Supporting Information), hs-PLA2 was found to dissociate from the bilayer surface heading for bulk water in the PLA2/DOPC system, while it remains bound to the bilayer surfaces in seven other systems. This is consistent with previous experimental research by Jain et al. that showed that phospholipase A2 hydrolyzes phospholipid vesicles in the

dx.doi.org/10.1021/bi3012687 | *Biochemistry* 2013, 52, 1477−1489

scooting mode[12−14] and hopping mode[14] for anionic and zwitterionic membranes, respectively. The phenomenon is also consistent with the experimental reports[28] that the ability of PLA2 to combine with phosphatidylcholine bilayers is weaker than that of anionic lipid bilayers. To obtain atomic details of the binding of the enzyme to bilayers, configurations from the CG−MD simulations were used as starting points for subsequent 120−160 ns all-atom MD simulations. This allowed us to investigate the accurate structural dynamics of the protein and lipid molecules.

METHODS

CG Simulations. The crystal structure of human synovial PLA2 [Protein Data Bank (PDB) entry 1POE, 2.1 Å resolution][10] was converted into a CG representation in which each amino acid is represented by one backbone bead whose Cartesian coordinates are just those of the Cα atom and several side particles whose Cartesian coordinates are determined using the literature.[29−31] The CG model was validated by comparing the potential of mean force for each amino acid as a function of its distance from the center of a dioleoylphosphatidylcholine (DOPC) bilayer with atomistic MD simulation results.[30] The CG model has been shown to be able to reproduce data derived from experiments and atomistic simulations for a number of membrane proteins and synthetic α-helical peptides.[30,32] The CG lipid model has also been shown to be able to reproduce structural properties of membranes derived from experiments.[29] The secondary and tertiary structures of PLA2 were restrained by an elastic network model (force constant of 10 kJ mol^{-1} Å^{2}) among all backbone particles that were within 7 Å of each other.[33]

Eight different CG−MD simulation systems were created (see Table 1). Six of them employed a mixed (2/3 SAPX/DOPX) bilayer, the lipid composition of which was set according to previous experimental[34] and computational[27] conditions. The initial configurations of CG−MD simulations were similar: one hs-PLA2 molecule placed in the center of the simulation box with dimensions of 9.6 nm × 9.6 nm × 9.6 nm, 128 phospholipid molecules randomly positioned around the hs-PLA2, and the simulation box solvated with 3000 CG water and counterions (Na^+ or Cl^-) to keep the system neutral. The system was then energy-minimized for 6000 steps with a steepest-descent algorithm, followed by a production MD simulation. Three simulations were performed for each system, with different velocities and initial coordinates of phospholipids. During the CG−MD simulations, we first used an anisotropic algorithm[35,36] for pressure coupling to change the box vectors in the *x*, *y*, and *z* directions, which help the phospholipids quickly assemble around the hs-PLA2 enzyme; after the lipid bilayer was successfully formed and the hs-PLA2 stayed on the surface of the lipid bilayer, we used a semi-isotropic algorithm[35,36] for pressure coupling with a simulation time of 2.5−3.2 μs to ensure that the final configuration of the CG−MD simulations corresponded to a local, or we hoped global, energy minimum. We extended the simulation time of all the eight systems to 8 μs in replicate CG simulations to observe the situation over a longer time.

All the simulations were conducted in the *NPT* ensemble, at a constant pressure of 1 bar and an absolute temperature of 310 K. The time step was 20 fs for all CG−MD simulations, and the pair list for computing nonbonded pair forces was updated every 10 steps with a list cutoff of 1.2 nm. The Coulombic and van der Waals interactions were computed using the shift algorithm, in which both the energy and force vanish at the cutoff distance (r_{cut}) of 1.2 nm. The electrostatic potential is shifted from an r_{shift} of 0.0 nm to r_{cut}. The Lennard-Jones (LJ) potential is shifted from an r_{shift} of 0.9 nm to r_{cut}. The weak coupling scheme of Berendsen and co-workers[35,36] was used for both temperature and pressure control, with the temperature coupling time constant of 1 ps. For pressure coupling, we used the coupling time constant of 5.0 ps and a compressibility of 4.5 × 10^{-5} bar^{-1}. The trajectory was collected every 20 ps, and all the simulations were performed with Gromacs version 4.4.5[37−40] in parallel under a Linux cluster.

All-Atom Simulations. Configurations at the end of the 2.5−3.2 and 8 μs CG−MD simulations were used as starting points for subsequent 120 and 160 ns all-atom MD simulations, respectively. Snapshots at the end of the CG−MD simulations were stripped of waters and counterions and transformed into all-atom structures based on the Charmm36 force field,[41−43] using the protocol proposed by Rzepiela et al.[44] Each mixture was then solvated with tip3p[45] water molecules and electrically neutralized by adding counterions. Each system was then energy-minimized for 10000 steps, using a steepest-descent algorithm, followed by an equilibration simulation of 1 ns with the *NVT* ensemble; then began the production all-atom MD simulation with the *NPT* ensemble.

All the simulations were performed at an absolute temperature of 310 K. For simulations under the *NPT* ensemble, a constant pressure of 1 bar was coupled. The time step was 2 fs for all simulations, and the pair list for computing nonbonded pair forces was updated every 10 steps with a list cutoff of 1.2 nm. The Coulombic and van der Waals interactions were computed using the cutoff algorithm, and the cutoff radii for both Coulomb and van der Waals interactions were 1.2 nm. The long-range electrostatic interaction was corrected using the particle mesh Ewald method[46,47] with a maximal spacing for the FFT grid of 0.16 nm and an interpolation order of 4. Bond lengths and angles were constrained using the LINCS algorithm.[48] The Nose-Hoover coupling scheme was used for temperature control,[49] with a temperature coupling time constant of 1.0 ps. A Parrinello-Rhaman barastat was used for semi-isotropic pressure coupling,[50] with a coupling time constant of 2.0 ps and a compressibility of 4.6 × 10^{-5} bar^{-1}. The trajectory was collected every 2 ps, and all the simulations were also performed with Gromacs version 4.4.5[37−40] in parallel under a Linux cluster.

RESULTS

The main academic question considered in this work is the mode of interaction of human synovial phospholipase A2 with different mixed lipid bilayers. To address the question, we analyzed the contact probability of all the amino acid residues in hs-PLA2 with the hydrophilic headgroups and hydrophobic acyl tails of lipid bilayers. On the basis of the statistical contact probability, we described the different aspects of hs-PLA2−bilayer interactions, including the penetration of hs-PLA2, contact of hs-PLA2 with the headgroups of lipid bilayers, hydrogen bonds between hs-PLA2 and lipid bilayers, secondary structure changes of hs-PLA2, and the influence of lipid molecules on the area of the entrance region of the hydrophobic binding pocket in hs-PLA2. Results from the 120 and 160 ns all-atom MD simulations are consistent. Without being explicitly stated, the results shown in this paper are those in the 120 ns simulation.

dx.doi.org/10.1021/bi3012687 | *Biochemistry* 2013, 52, 1477−1489

Table 2. Amino Acid Residues That Penetrate into the Hydrophobic Area of Lipid Bilayers in Different Simulated Systems and Distances between the Centers of Mass of These Amino Acid Residues and the Centers of Mass of Lipid Bilayers (angstroms)

PLA2/DOPC	Leu2	Val3	Leu19	Phe23	Val30
	23.08	23.48	21.81	21.56	21.66
	Lys62	Phe63	Gln110	Tyr111	His47
	20.97	20.87	19.94	18.50	31.52
PLA2/DOPE	Val3	Ala18	Leu19	Phe23	Lys62
	21.46	19.97	19.74	21.30	19.87
	Phe63	Tyr111	His47		
	19.27	21.26	31.2		
PLA2/SAPE/DOPC	Leu2	Leu19	Gly22	Phe23	Val30
	22.00	17.06	19.98	18.21	21.89
	Gln110	Tyr111	His47		
	17.69	17.26	32.32		
PLA2/SAPE/DOPE	Leu2	Leu19	Phe23	Val30	Phe63
	22.09	23.41	24.84	21.23	19.48
	Tyr111	His47			
	22.28	30.21			
PLA2/SAPG/DOPC	Leu2	Val3	Ala18	Leu19	Phe23
	20.25	18.72	18.61	18.03	16.87
	Val30	Phe63	Tyr111	Ser113	His47
	16.64	18.43	14.31	19.18	27.77
PLA2/SAPG/DOPE	Val3	Leu19	Phe23	Val30	Lys62
	20.41	19.89	20.11	19.36	19.37
	Phe63	His47			
	17.10	30.16			
PLA2/SAPM/DOPC	Leu2	Val3	Ala18	Leu19	Gly22
	19.70	17.04	19.91	17.78	22.61
	Phe23	Val30	Phe63	Tyr111	His47
	20.12	19.51	16.62	18.94	28.69
PLA2/SAPM/DOPE	Leu2	Val3	Leu19	Phe23	Val30
	22.04	21.62	21.12	21.59	20.68
	Lys62	Phe63	Tyr111	His47	
	20.07	17.91	19.21	29.47	

Penetration of the Protein. To assess the penetration of hs-PLA2 into mixed lipid bilayers, we calculated the minimal distance (D_{min}) between every amino acid residue of hs-PLA2 and the acyl tails (all except the first carbon atoms in the *sn*-1 and *sn*-2 tails) of lipid bilayers at every recorded simulation step and counted the number of D_{min} values that were <3.5 Å as the contact number of each amino acid residue. If the contact number of an amino acid residue is larger than 75% of the total recorded simulation step in the analyzed trajectory, we define the amino acid residue as one that has penetrated into the hydrophobic area of lipid bilayers. Table 2 lists the amino acid residues penetrating into the hydrophobic area of lipid bilayers in all the simulated systems and the average distances between the center of mass of each amino acid residue and the center of mass of the lipid bilayer in the *z* direction. In Table 2, we show that hydrophobic residues Leu2, Val3, Ala18, Leu19, Phe23, Gly30, and Phe63 that form the edge of the entrance of the hydrophobic binding pocket in hs-PLA2 tend to make contact with the acyl tails of lipid bilayers, which is in accordance with previous experimental results.[9] Gln110 and Tyr111, which are placed near the hydrophobic binding pocket of hs-PLA2, are also prone to penetration into the hydrophobic area of lipid bilayers and help anchor hs-PLA2 at the surface of lipid bilayers, as shown in Figure 1. For a selected lipid component, these amino acid residues penetrate deeper into the hydrophobic area when the lipid component is mixed with DOPC molecules to form a lipid bilayer, and the penetration depth would be smaller if the lipid component were mixed with DOPE molecules. For example, in the hs-PLA2/SAPE/DOPC system, the average distance between the penetrating amino acid residues and the bilayer center in the *z* direction is 19.16 Å, while the value in the hs-PLA2/SAPE/DOPE system is 22.22 Å; the situation is similar in the bilayers that include SAPG and

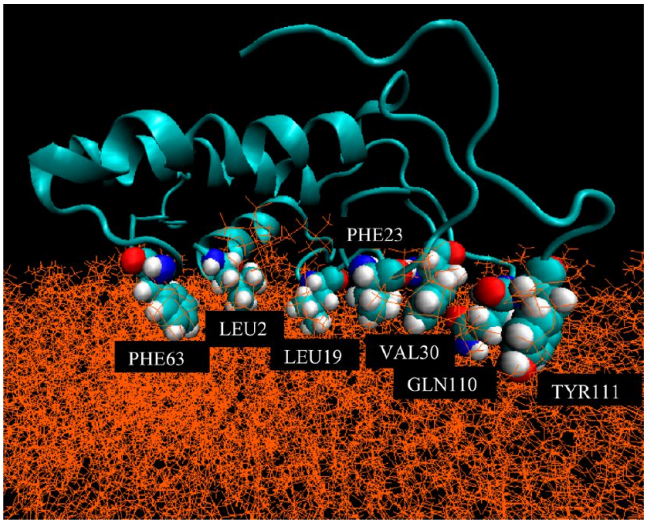

Figure 1. Amino acid residues penetrating into the lipid bilayer in the hs-PLA2/DOPC system.

dx.doi.org/10.1021/bi3012687 | *Biochemistry* 2013, 52, 1477−1489

SAPM molecules. This is easy to understand as DOPC has a larger area per lipid molecule than DOPE, which makes it easier for hydrophobic amino acid residues in hs-PLA2 to penetrate into lipid bilayers.

To further demonstrate the relative location of amino acid residues that penetrate into the hydrophobic area of lipid bilayers, we calculated the number density distributions of the penetrating amino acid residues, the phosphorus atoms, and the glycerol backbone of lipid bilayers along the membrane normal. The results for the eight systems are shown in Figure 2. As can

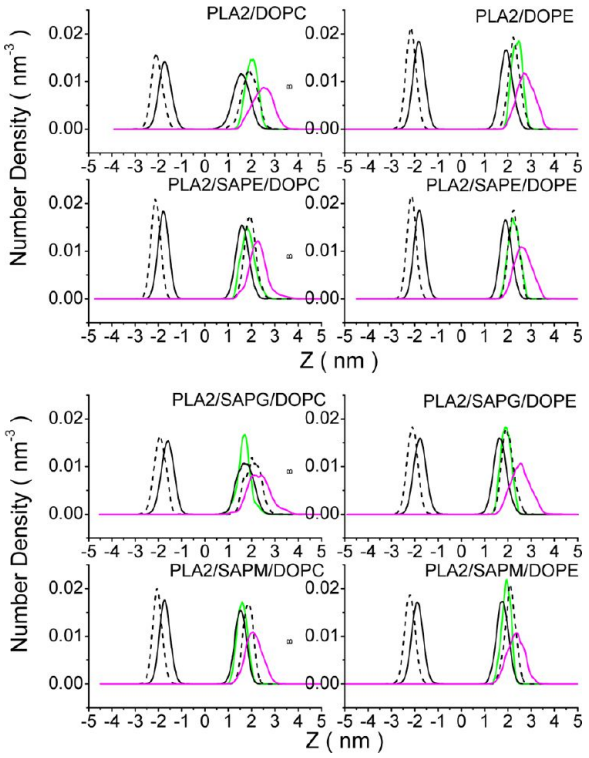

Figure 2. Normalized number density profiles of several components along the membrane normal in eight simulated systems: green for amino acid residues penetrating into lipid bilayers in hs-PLA2, red for amino acid residues making contact with hydrophilic headgroups in lipid bilayers in hs-PLA2, black for phosphorus atoms in lipid molecules, and black dashed for the glycerol backbone in lipid molecules. The number densities of amino acid residues are multiplied by a factor of 10 for the sake of clarity.

be seen in the figure, in all eight systems these amino acid residues stay between the glycerol backbone and phosphorus atoms of lipid bilayers. The peak value of the number density distribution of penetrating amino acid residues is located closer to the center of bilayers composed of anionic lipid molecules. For example, in the PLA2/SAPE/DOPC system, the peak value of the number density distribution of penetrating amino acid residues is located at 18.50 Å and is located at 16.91 Å in the PLA2/SAPG/DOPC system. We also find that these amino acid residues would penetrate deeper into the hydrophobic area if the lipid bilayer had DOPC molecules as a component in comparison with the situation when the lipid bilayer includes DOPE. For example, in the PLA2/SAPE/DOPC system, the peak value of the number density distribution of penetrating amino acid residues is located at 18.50 Å and is located at 22.38 Å in the PLA2/SAPE/DOPE system, and the situation is similar in the other six systems.

We also computed the variation of the bilayer thickness with respect to the distance from the hs-PLA2 center. The results and algorithm are shown in Figure S3 of the Supporting Information. As can be seen, when phospholipids are within 1 nm fo the hs-PLA2 center, they stay in the hydrophobic pocket of hs-PLA2 and tend to have a higher position in the z direction; thus, the bilayer thicknesses are larger. When phospholipids are within 1−3 nm of the PLA2 center, they interact with amino acid residues in hs-PLA2 and the positions of phospholipids are strongly influenced; thus, the bilayer thicknesses are quite irregular. When phospholipids are more than 3 nm from the hs-PLA2 center, they are less affected by amino acid residues in hs-PLA2; thus, the bilayer thicknesses are more stable than those in the situation in which phospholipids stay close to the hs-PLA2 center. According to our analysis in Table S1 of the Supporting Information, bilayers containing anionic phospholipids are more likely to make contact with amino acid residues in hs-PLA2 in the aqueous interface; thus, the thickness of bilayers containing anionic phospholipids has an upward trend at distances from the hs-PLA2 center of >1 nm.

In addition, we defined the average bilayer thickness as the distance between the average z coordinate of phosphorus atoms in the upper and lower bilayer leaflet. On the basis of the same Charmm force field,[41−43] we calculated the average bilayer thickness for (1) lipid bilayers when hs-PLA2 binds to them and (2) pure lipid bilayers in excess water (the simulation time for pure lipid bilayers is 120 ns). The results are listed in Table 3; from these results, we find that the presence of hs-PLA2 slightly decreases the bilayer thickness, compared to those of pure lipid bilayers.

Table 3. Thicknesses of Lipid Bilayers in the Presence and Absence of hs-PLA2

	DOPC	DOPE	SAPE/DOPC	SAPE/DOPE
thickness of bilayer with PLA2 (nm)	3.99 ± 0.05	4.49 ± 0.05	4.25 ± 0.07	4.35 ± 0.05
thickness of pure bilayer (nm)	4.16 ± 0.06	4.50 ± 0.05	4.38 ± 0.06	4.56 ± 0.06
	SAPG/DOPC	SAPG/DOPE	SAPM/DOPC	SAPM/DOPE
thickness of bilayer with PLA2 (nm)	3.97 ± 0.05	4.21 ± 0.09	4.10 ± 0.06	4.30 ± 0.07
thickness of pure bilayer (nm)	4.22 ± 0.06	4.48 ± 0.08	4.34 ± 0.07	4.52 ± 0.04

Protein−Lipid Interaction. To have a more detailed description of human synovial PLA2−lipid bilayer interactions, we calculated the contact probability of all 124 amino acid residues with the headgroups of the bilayer surface using the same method that is described above. Some of the results are displayed in Figures 3 and 4, and the overall data can be found in Tables S1 and S2 of the Supporting Information. In Figure 3, we show the probability of the amino acids forming the hs-PLA2 binding pocket entrance in contacting the headgroups of the whole lipid bilayer. Here we refer to the headgroup of a lipid as the molecule without the alkyl groups of the two acyl tails. From Figure 3, we can see that the amino acid sequences of the entrance of the hydrophobic binding pocket are more likely to make contact with bilayers containing SAPE, SAPG, or SAPM molecules than pure DOPC and DOPE bilayers. It is in

dx.doi.org/10.1021/bi3012687 | *Biochemistry* 2013, 52, 1477−1489

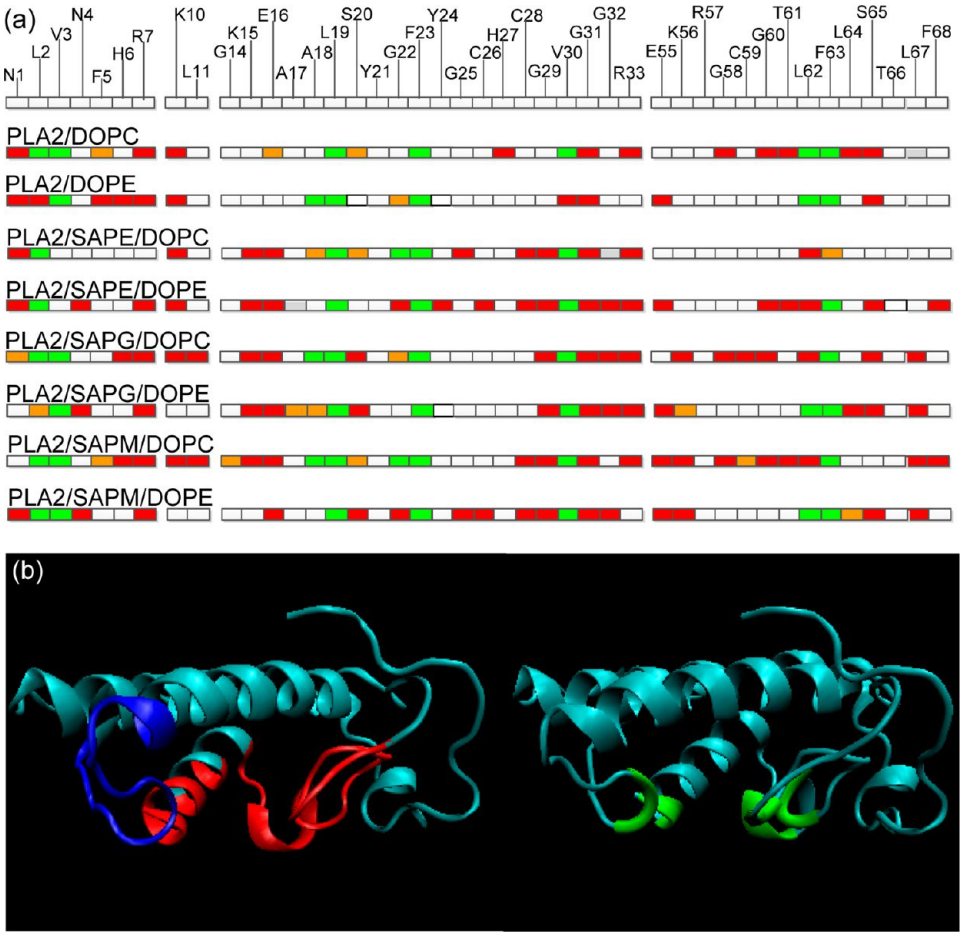

Figure 3. (a) Amino acid sequences of the entrance of the binding pocket in human synovial phospholipase A2. Green blocks stand for amino acids that penetrate into lipid bilayers; red (>90%) and orange (75−90%) blocks stand for amino acids making contact with the headgroups of lipid bilayers with different probabilities. (b) Entrance of the binding pocket in human synovial phospholipase A2: red for Asn1−Arg7, Lys10, Leu11, Gly14−Arg33, and Glu55−Phe68 and green for amino acid residues in the entrance of the binding pocket that penetrate into lipid bilayers (Leu2, Val3, Ala18, Leu19, Gly22, Phe23, Val30, Leu62, and Phe63).

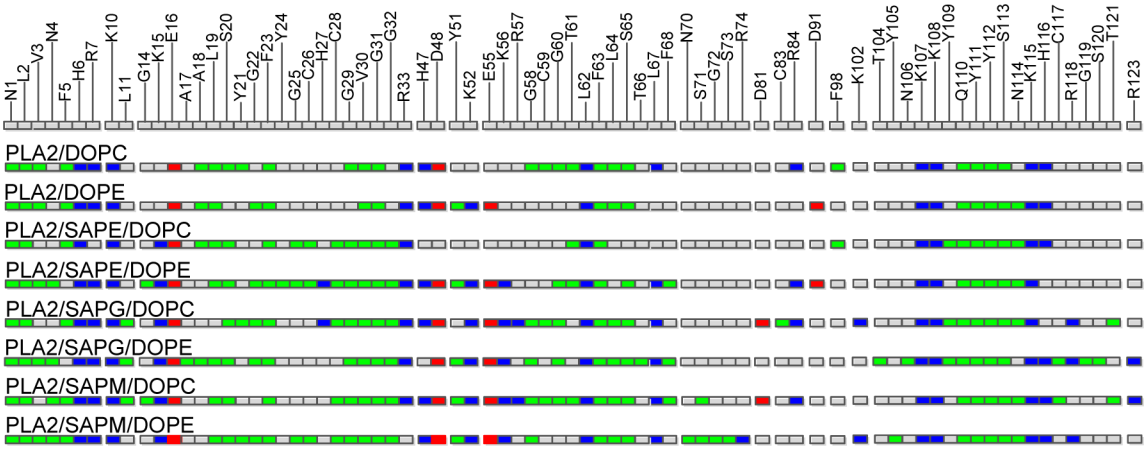

Figure 4. Amino acid sequences of the entrance of the hydrophobic binding pocket (Asn1−Arg7, Lys10, Leu11, Gly14−Arg33, and Glu55−Phe68) and random coil (Lys102−Gly119) of human synovial phospholipase A2. Green blocks stand for amino acids with neutral side chains that make contact with the headgroups of lipid bilayers; blue and red blocks stand for amino acids with basic and acidic side chains, respectively, making contact with the headgroups of lipid bilayers.

accordance with previous conclusions that hs-PLA2s destabilize and desolvate lipid molecules when binding to the surface of biomembranes,[51,52] and hs-PLA2 tends to interact with the anionic membrane surface because of positively charged basic amino acid residues on the interfacial recognition site of hs-PLA2.[53] We also find that amino acid residues close to residues Leu19, Phe23, Val30, and Phe63, namely, Ala18, Ser20, Gly22, Gly29, Gly31, Gly32, Arg33, Gly60, Thr61, Lys62, Leu64, and

dx.doi.org/10.1021/bi3012687 | *Biochemistry* 2013, 52, 1477−1489

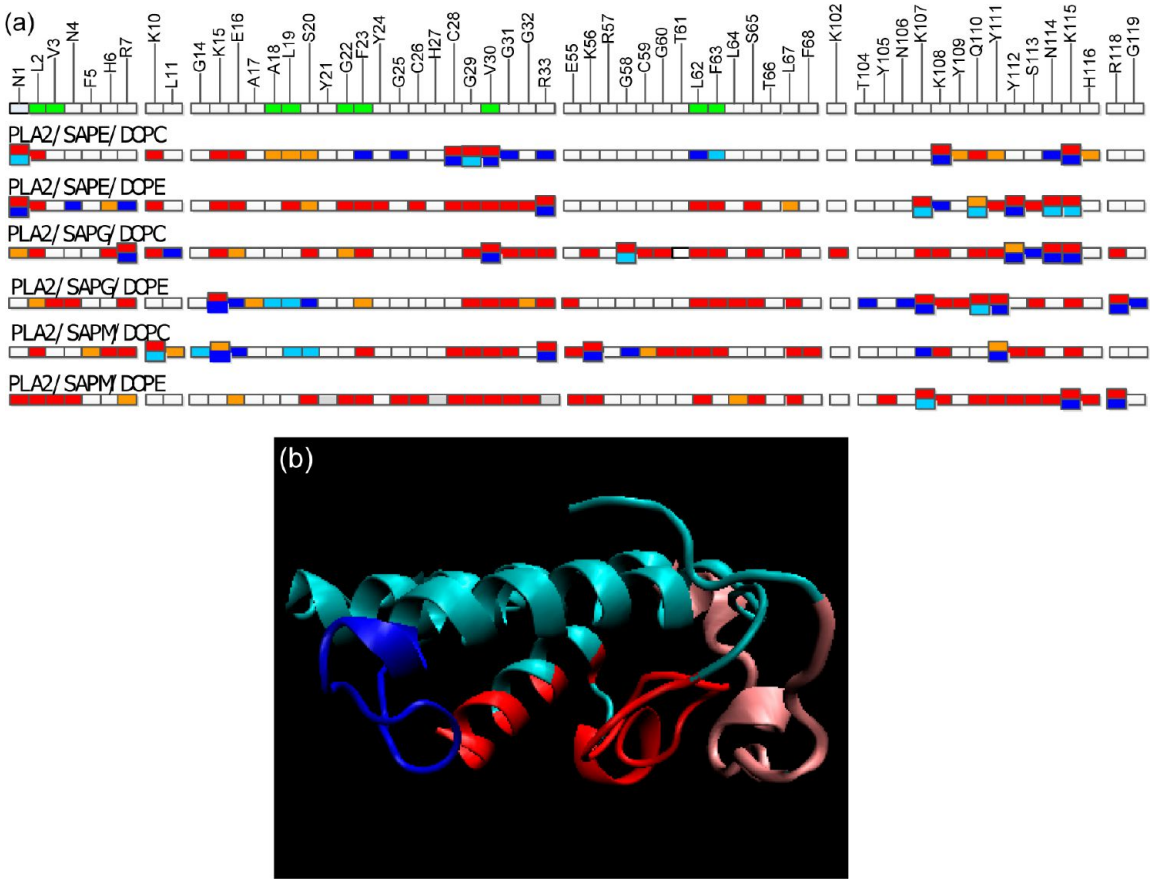

Figure 5. (a) Amino acid sequences of the entrance of the binding pocket (Asn1−Arg7, Lys10, Leu11, Gly14−Arg33, and Glu55−Phe68) and random coil (Lys102−Gly119) of human synovial phospholipase A2. Green blocks stand for amino acids that penetrate into lipid bilayers and form the entrance of the binding pocket of hs-PLA2; red (>90%) and orange (75−90%) blocks stand for amino acids making contact with the headgroups of SAPE, SAPG, or SAPM molecules with different probabilities. Blue (>90%) and sky blue (75−90%) blocks stand for amino acids making contact with the headgroups of DOPC or DOPE molecules with different probabilities. (b) Depiction of the entrance of the binding pocket of human synovial phospholipase A2 (red for Asn1−Arg7, Lys10, Leu11, and Gly14−Arg33 and blue for Glu55−Phe68) and the random coil of human synovial phospholipase A2 (pink for Lys102−Gly119).

Ser65, tend to make contact with the headgroups of lipid bilayers. This is easy to understand because these residues penetrate into the hydrophobic area of lipid bilayers; amino acid residues nearby would be more likely to make contact with lipid headgroups.

To gain a clear view of the category of amino acid residues making contact with the headgroups of lipid bilayers, we classified the amino acid residues with contacting probabilities of >45% into five species, and these results can be found in Table S2 of the Supporting Information. The contact probabilities of amino acid residues with neutral, basic, or acidic side chains are displayed in Figure 4, which shows that the majority of amino acid residues making contact with the headgroups of lipid bilayers were neutral amino acids with aliphatic, aliphatic hydroxyl, or sulfur-containing side chains, and the second largest group of contacting amino acid residues consists of positively charged basic amino acids. For bilayers composed of zwitterionic lipid molecules, bilayers containing DOPC are slightly more likely to make contact with amino acid residues with basic side chains and less likely to make contact with amino acid residues with acidic side chains. For bilayers composed of anionic lipid molecules (SAPG and SAPM), the probability of lipid headgroups making contact with basic side chains increases. In the PLA2/SAPG/DOPC system, 18 amino acid residues with basic side chains make contact with bilayer headgroups with a probability of >45%, and in the PLA2/SAPG/DOPE system, 16 amino acid residues reach the same standard.

To gain a clear understanding of the competition of different lipid molecules making contact with hs-PLA2, we analyzed the probability of amino acid residues making contact with different species of lipid molecules in hs-PLA2/mixed bilayer systems. The results are listed in Table S3 of the Supporting Information and transformed into a more intuitive way of being expressed in Figure 5. We can see from Figure 5 that, for bilayers including anionic lipid molecules (SAPG and SAPM), amino acid residues mostly make contact with these negatively charged lipids; for bilayers composed of zwitterionic lipids, DOPC molecules are more competitive than DOPE molecules in interacting with hs-PLA2. In the hs-PLA2/SAPE/DOPC system, amino acid residues have almost equal probability of making contact with SAPE and DOPC molecules, while in the hs-PLA2/SAPE/DOPE system, amino acid residues make contact with SAPE molecules with a much higher probability than DOPE. Amino acid residues making contact with lipid bilayers mainly are located around the entrance of the binding pocket in hs-PLA2, which is formed by hydrophobic amino acid residues Leu2, Val3, Ala18, Leu19, Gly22, Phe23, Val30, Leu62, and Phe63. Amino acid residues from Lys102 to Cys124 at the C-terminus of hs-PLA2 are also found to make contact with

dx.doi.org/10.1021/bi3012687 | *Biochemistry* 2013, 52, 1477−1489

Table 4. Average Numbers of Hydrogen Bonds per Time Step for Each Group in Simulated Systems

	PLA2/DOPC	PLA2/DOPE	PLA2/SAPE/DOPC	PLA2/SAPE/DOPE
total	19.333	24.107	19.302	28.355
phosphate	19.039	17.454	15.779	17.390
glycerol backbone	0.001	0.002	0.040	0.017
carbonyl	0.293	3.039	2.008	2.944
amine		3.612	1.475	8.004
	PLA2/SAPG/DOPC	PLA2/SAPG/DOPE	PLA2/SAPM/DOPC	PLA2/SAPM/DOPE
total	37.073	32.258	35.832	35.205
phosphate	23.540	23.248	28.674	24.471
glycerol backbone	0.108	0.008	0.046	0.901
carbonyl	9.062	2.997	3.862	3.645
glycerol or mythelene glycol	4.363	4.480	3.250	5.624
amine		1.525		0.564

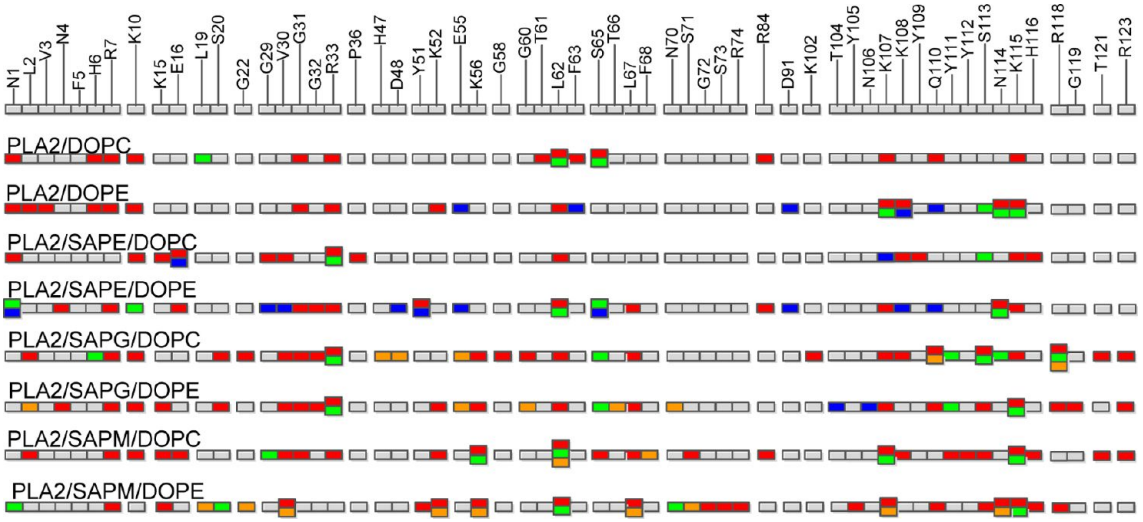

Figure 6. Amino acid residues in hs-PLA2 forming hydrogen bonds with phosphate (red), carbonyl (green), amine (blue), or glycerol or methylene glycol (orange) groups in various lipid bilayers with probabilities of >25%.

lipid headgroups. It can be found in Figure 5 that the entrance of the hydrophobic binding pocket in hs-PLA2 mainly makes contact with SAPE, SAPG, and SAPM molecules, whereas DOPC and DOPE molecules tend to make contact with the random coil from Lys102 to Cys124 at the C-terminus of hs-PLA2. This phenomenon is very obvious in SAPG- and SAPM-containing bilayers. According to the analysis described above, lipid molecules with an arachidonoyl *sn*-2 chain are more competitive in making contact with hs-PLA2, which is in accordance with the fact that arachidonic acid is an important hydrolysis product of hs-PLA2.[54,55]

Hydrogen Bonds. We analyzed the average number of hydrogen bonds formed between hs-PLA2 and the headgroups of lipid bilayers per time step over the simulation time. The results are listed in Table 4. The data suggest that a total of 19–38 hydrogen bonds formed between PLA2 and the lipid bilayers, most of which formed with the phosphate groups of lipid bilayers. In bilayers composed of zwitterionic lipids, the existence of DOPE molecules would increase the number of hydrogen bonds between the protein and bilayers, while in bilayers composed of anionic lipids, the presence of DOPC molecules would aid in the formation of more hydrogen bonds. To interpret the phenomenon, we calculated the probability of all the amino acid residues in hs-PLA2 forming hydrogen bonds with a phosphate, glycerol backbone, carbonyl, amine, glycerol, or methylene glycol group in various lipid bilayers. The results are listed in Table S4 of the Supporting Information. Amino acid residues forming hydrogen bonds with phosphate (red), carbonyl (green), amine (blue), or glycerol or methylene glycol (orange) groups in various lipid bilayers with probabilities higher than 25% are shown in Figure 6. As can be seen in the figure, compared with the choline groups in the hs-PLA2/DOPC system, the amine headgroups in the hs-PLA2/DOPE system form hydrogen bonds with Glu55, Phe63, Asp91, Lys108, and Gln110, which leads to the increment of hydrogen bonds between hs-PLA2 and the carbonyl headgroups in DOPE molecules. The same situation exists in hs-PLA2/SAPE/DOPC and hs-PLA2/SAPE/DOPE systems. Thus, we conjectured that for bilayers composed of zwitterionic lipids, the amine groups in DOPE molecules form hydrogen bonds with hs-PLA2, which leads to the concatenate effect of the carbonyl groups forming hydrogen bonds with hs-PLA2 and the total number of hydrogen bond increases. However, for bilayers containing anionic phospholipids that have stronger electrostatic interaction with hs-PLA2 than DOPE molecules, amino acid residues mostly form hydrogen bonds with the phosphate and carbonyl groups in anionic lipids. Addition of DOPE molecules would increase the number of hydrogen bonds of hs-PLA2 with the amine groups in DOPE molecules and the glycerol or methylene glycol groups in SAPG/SAPM molecules, which leads to the decrease in the number of hydrogen bonds of hs-PLA2 with the phosphate or carbonyl

dx.doi.org/10.1021/bi3012687 | *Biochemistry* 2013, 52, 1477–1489

groups in anionic lipids, and the total number of hydrogen bond decreases.

Changes in the Secondary Structure of the Protein. To address the influence of lipid composition on the secondary structure of hs-PLA2, we fit the whole protein structure to the crystal structure of Protein Data Bank entry 1POE (rotation and translation) and calculated the root-mean-square deviation (rmsd) of every amino acid residue in hs-PLA2 over the atomic MD simulations. Figure 7 shows the rmsd of every amino acid

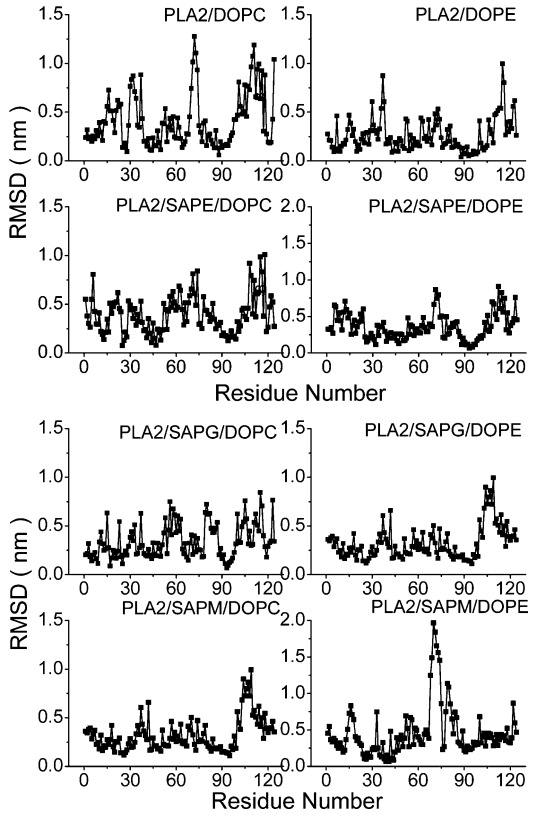

Figure 7. Root-mean-square deviations (rmsds) of every amino acid residue in hs-PLA2 during the atomic MD simulations in eight systems.

residue in hs-PLA2 in all the systems simulated. We can see from the figure that in the eight systems simulated, residues Val30−Thr40, Tyr66−Gln80, and Lys107−Arg118 have relatively large rmsds compared to the Protein Data Bank crystal structure during the simulation time. Taking the PLA2/DOPC system as an example, we draw the crystal structure of hs-PLA2 in the Protein Data Bank and the structure at the end of the atomic simulation in Figure 8, coloring residues Val30−The40, Tyr66−Gln80, and Lys107−Arg118 red, blue, and yellow, respectively. Using Figures 7 and 8, we find that residues 30−40 (red) have a large root-mean-square deviation, which is in agreement with the observed enlargement of the entrance region of the hydrophobic binding pocket. We also find that the sequential residues Tyr66−Gln80 (blue) have an obviously larger root-mean-square deviation than surrounding residues. The antiparallel β-sheet is even broken into random coil structure (Figure 8). Besides, coil residues Lys107−Arg118 (yellow) also change their structures after PLA2 binds to the surface of the lipid bilayer: hydrophobic residues Gln110 and Tyr111 embed in the lipid bilayer, which stabilizes the coil on the bilayer surface; Ser113−His116 tend to interact with the lipid headgroups and thus move upward instead of staying in the hydrophobic area of the bilayer, which also leads to large rmsds. These large changes result from the interaction of amino acid residues with the hydrophilic headgroups of the DOPC bilayer and are preconditions to the proper function of the enzyme.

To further prove our results, the rmsds of every amino acid residue in hs-PLA2 in the 120 and 160 ns all-atom MD simulations are displayed in Figure S3 of the Supporting Information, from which we find that the magnitudes of the rmsds of every amino acid residue in both atomic MD simulations are consistent.

Area of the Hydrophobic Binding Pocket. hs-PLA2 hydrolyzes lipids by capturing lipid molecules in its hydrophobic binding pocket, where His47 catalyzes the hydrolysis of the *sn*-2 ester bond of lipid molecules. To understand the influence of bilayer composition on the configuration of the hydrophobic binding pocket of hs-PLA2, we calculated the area and width of the entrance region of the hs-PLA2 hydrophobic binding pocket in the eight studied systems. For all the systems simulated, Leu19, Phe23, Val30, and Phe63 formed the edge of the entrance of the hs-PLA2 hydrophobic binding pocket and tended to penetrate into the hydrophobic area of lipid bilayers. We projected the four amino acids onto the $x-y$ plane and calculated the area of the quadrangle to represent the area of the entrance region of the hydrophobic binding pocket. Shown in Figure S4 of the Supporting Information is an example to illustrate the quadrangle formed by the four amino acid residues in the case of the hs-PLA2/SAPE/DOPC system. To enter the hydrophobic binding pocket, a lipid molecule needs to pass through the region between Val30 and Phe63; thus, we define the distance between the projected center of Val30 and Phe63 on the $x-y$ plane as the width of the binding pocket. We calculated the average area and width of the entrance region of the hydrophobic binding pocket in each system during the last 40 ns of simulation time and listed the results in Table 5. From Table 5, we find that the areas of the entrance region of the hydrophobic binding pocket in hs-PLA2/bilayer systems are much larger than the area in the crystal structure of the Protein Data Bank, which indicates that lipid molecules can adjust the structure of the functional segments of hs-PLA2 in the cellular process. For mixed lipid bilayers, the area of the entrance region of the hydrophobic binding pocket would be larger when DOPC is included in the lipid bilayer. For example, in the hs-PLA2/SAPE/DOPC system, the area is 1.75 nm^2, while this value is 1.42 nm^2 in the PLA2/SAPE/DOPE system. To explain the results, we turn to the boundaries of the binding pocket defined by amino acid residues Leu19, Phe23, Val30, and Phe63, together with other abutting residues. These amino acid residues interact quite strongly with the lipid molecules of a bilayer surface, and the total molecular area of the contacting lipid molecules governs the area of the binding pocket in hs-PLA2. In comparison with DOPE, DOPC molecules have a higher fluidity and a larger molecular area at a given temperature; thus, replacing DOPE with DOPC as contacting lipids might increase the area of the binding pocket in hs-PLA2. We can see from Figure 5 that, in the PLA2/SAPE/DOPC system, amino acid residues Leu23, Cys28, Gly29, Val30, Gly31, Arg33, Lys62, and Phe63 mostly make contact with DOPC molecules while, in the PLA2/SAPE/DOPE system, they tend to make contact with SAPE molecules; because DOPC molecules have a larger molecular area than SAPE molecules,[56] the area of the binding pocket is larger in the

dx.doi.org/10.1021/bi3012687 | *Biochemistry* 2013, 52, 1477−1489

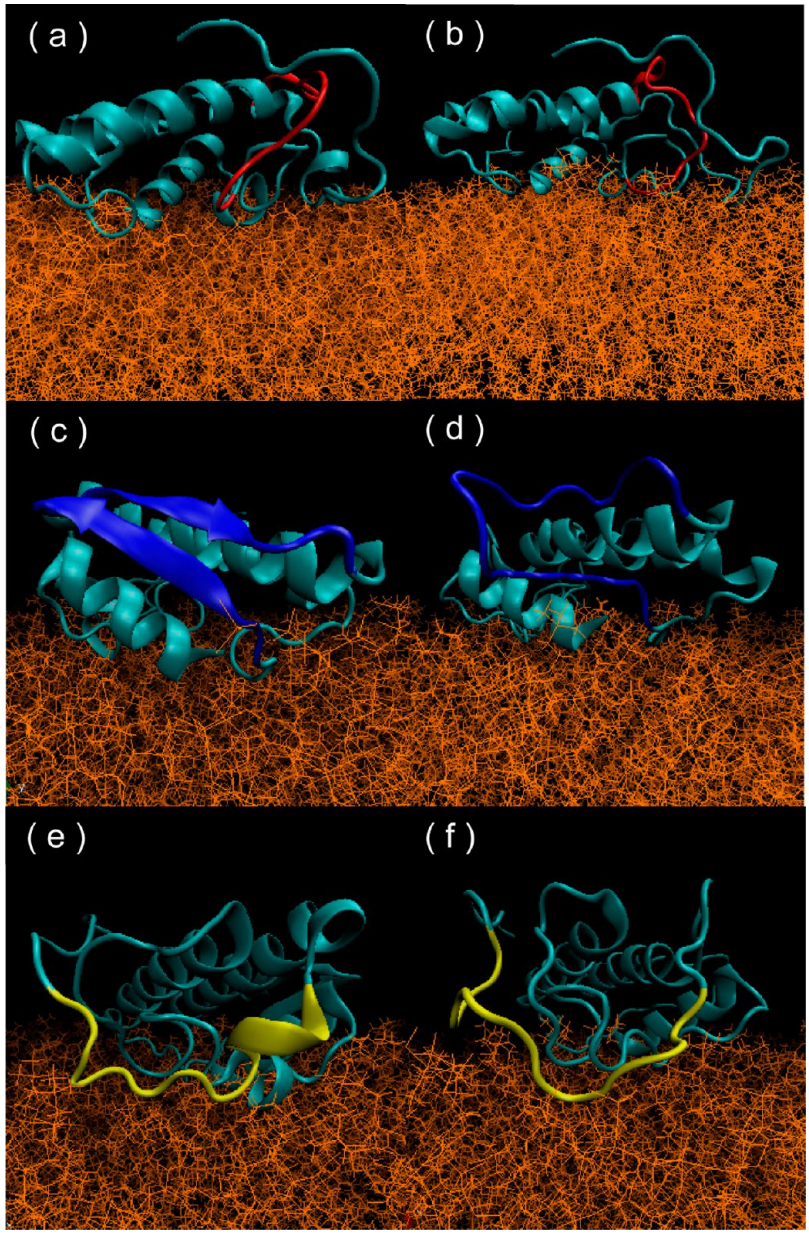

Figure 8. Structures of hs-PLA2 in the Protein Data Bank (left) and at the end of the simulation for the hs-PLA2/DOPC system (right): red for Val30−Thr40, blue for Tyr66−Gln80, and orange for Lys107−Arg118.

Table 5. Areas and Widths of the Entrance Region of the Hydrophobic Binding Pocket in hs-PLA2 Obtained from All-Atom MD Simulation Trajectories and from the Crystal Structure of PDB entry 1POE

	crystal structure	PLA2/DOPC	PLA2/DOPE
area (nm^2)	0.96	1.51 ± 0.10	1.32 ± 0.07
width (nm)	1.25	2.18 ± 0.04	1.64 ± 0.08
	PLA2/SAPE/DOPC	PLA2/SAPE/DOPE	PLA2/SAPG/DOPC
area (nm^2)	1.75 ± 0.14	1.42 ± 0.10	1.45 ± 0.09
width (nm)	2.11 ± 0.09	1.73 ± 0.08	1.91 ± 0.06
	PLA2/SAPG/DOPE	PLA2/SAPM/DOPC	PLA2/SAPM/DOPE
area (nm^2)	1.40 ± 0.07	1.37 ± 0.09	1.32 ± 0.10
width (nm)	1.43 ± 0.08	1.69 ± 0.11	1.47 ± 0.08

PLA2/SAPE/DOPC system than in the PLA2/SAPE/DOPE system.

With respect to the influence of different negatively charged lipids on the area of the hs-PLA2 binding pocket, we think the area of a single lipid molecule, which can also be represented by fluidity, plays an important role. Because SAPG molecules are more fluid and possess a larger area per molecule than SAPM molecules,[56,57] hs-PLA2 making contact with bilayers contain-

dx.doi.org/10.1021/bi3012687 | *Biochemistry* 2013, 52, 1477−1489

ing SAPG tends to have a larger binding pocket area than when it makes contact with bilayers containing SAPM. To further prove our results, we list the areas and widths of the hs-PLA2 binding pocket in the 160 ns all-atom MD simulation in Table S5 of the Supporting Information. The data show that bilayers containing DOPC lead to larger areas and widths in hs-PLA2 compared to those of bilayers containing DOPE. In addition, from the analysis of rmsds of amino acid residues in Figure 7, we find that the rmsds of the four amino acid residues (Leu19, Phe23, Val30, and Phe63) are larger in bilayers containing DOPC than in those containing DOPE, which is in accordance with our conclusion.

DISCUSSION

Although the membrane-bound human synovial PLA2 has been studied by molecular dynamics simulations previously,[22] some important aspects of protein−membrane interactions, such as the credible penetration depth, the reliable contact between amino acid residues and lipid headgroups, and the conformational change in the protein on membrane surfaces, have not been studied readily because of the large size, the complexity of the system, and the limitation of simulation time. In this study, we utilized the efficiency of the CG model extending the simulation time to up to 3.2 μs and investigated the fully equilibrated complexes of hs-PAL2 with different types of lipid bilayers. Several conclusions can be drawn form our simulation results. hs-PLA2 tends to stay on the surface of lipid bilayers; hydrophobic residues Leu2, Val3, Ala18, Leu19, Phe23, Val30, and Phe63 that form the entrance of the hydrophobic binding pocket in hs-PLA2 tend to make contact with the acyl tails of lipid bilayers and stay between the glycerol backbone and phosphorus atoms of lipid bilayers. More than half of the total amino acid residues of hs-PLA2 make contact with the headgroups of lipid molecules (Table S1 of the Supporting Information), most of which are neutral amino acids with aliphatic, aliphatic hydroxyl, or sulfur-containing side chains, and the second largest group of contacting amino acid residues consists of positively charged basic amino acids. For the mixed bilayers, hs-PLA2 prefers to interact with lipid molecules that possess negative charge or more fluidity at the same temperature (Table S3 of the Supporting Information). Analysis of hydrogen bonds shows that a total of 19−38 hydrogen bonds form between hs-PLA2 and lipid bilayers, most of which are with the phosphate groups of lipid bilayers. The number of amino acid residues that form hydrogen bonds is much smaller than the number of amino acid residues that make contact with lipid bilayers (Tables S1 and S4 of the Supporting Information), which indicates that other effects, such as hydrophobic and electrostatic interactions, are important modes of interaction between hs-PLA2 and lipid bilayers. For bilayers including DOPC, because DOPC is more fluid and has a larger molecular area than DOPE, contact with DOPC molecules leads to larger rmsds and larger areas and widths of the hydrophobic binding pocket in hs-PLA2 than in cases of contact with DOPE molecules. This phenomenon can be considered as an illustration to the influence of bilayer fluidity on the structure of membrane-associated proteins.

In summary, we have conducted series of combined coarse-grain and all-atom MD simulations on eight hs-PLA2/bilayer systems; the coarse-grained simulation time is sufficient to find the complexes of hs-PLA2 on model membranes with low free energy, and the all-atom MD simulations are beneficial for the investigation of the atomic details of hs-PLA2−bilayer interaction modes and the structural changes of hs-PLA2 on model membranes. The conclusions drawn from our study might be helpful in understanding the detailed model of interactions between hs-PLA2 or other membrane-associated proteins and the lipid−water interface. The simulation method proposed in this work provides an alternative approach for modeling the larger-scale structures that are involved in membrane bilayers.

ASSOCIATED CONTENT

Supporting Information

Longer CG simulations (Figures S1 and S2), variation of the bilayer thickness with respect to the distance from the hs-PLA2 center (Figure S3), rmsds of every amino acid residue in hs-PLA2 over the 120 and 160 ns all-atom MD simulations (Figure S4), illustration of the area of the entrance region of the hydrophobic binding pocket (Figure S5), probability distribution, categorization, competition, and hydrogen bond distribution of amino acid residues making contact with the headgroups of lipid bilayers (Tables S1−S4, respectively), and areas and widths of the hydrophobic binding pocket in hs-PLA2 in the 160 ns all-atom MD simulations (Table S5). This material is available free of charge via the Internet at http://pubs.acs.org.

AUTHOR INFORMATION

Corresponding Author

*Telephone: (+86) 10 6279 2492. Fax: (+86) 10 6277 1149. E-mail: yuzhw@tsinghua.edu.cn.

Funding

This work was supported by grants from the Natural Science Foundation of China (Grants 21133009 and 21176132).

Notes

The authors declare no competing financial interest.

ACKNOWLEDGMENTS

We are grateful to Prof. Zhigang Shuai for computation resource support.

ABBREVIATIONS

PLA2, phospholipase A2; hs-PLA2, human synovial phospholipase A2; sPLA2, secretory phospholipase A2; cPLA2, cytosolic phospholipase A2; rmsd, root-mean-square deviation; CG, coarse-grained; MD, molecular dynamics; DLPE, dilaurylphosphatidylethanolamine; DOPC, dioleoylphosphatidylcholine; DOPE, dioleoylphosphatidylethanolamine; SAPE, 1-stearoyl-2-arachidonoyl-*sn*-glycero-3-phosphatidylethanolamine; SAPG, 1-stearoyl-2-arachidonoyl-*sn*-glycero-3-phosphatidylglycerol; SAPM, 1-stearoyl-2-arachidonoyl-*sn*-glycero-3-phosphatidylmethylene glycol; POPG, 1-palmitoyl-2-oleoyl-*sn*-glycero-3-phosphatidylglycerol; POPC, 1-palmitoyl-2-oleoyl-*sn*-glycero-3-phosphatidylcholine.

REFERENCES

(1) Schaloske, R. H., and Dennis, E. A. (2006) The phospholipase A2 superfamily and its group numbering system. *Biochim. Biophys. Acta 1761*, 1246−1259.

(2) Boegeman, S. C., Deems, R. A., and Dennis, E. A. (2004) Phospholipid Binding and the Activation of Group IA Secreted Phospholipase A2. *Biochemistry 43*, 3907−3916.

(3) Reed, K. A., Tucker, D. E., Aloulou, A., Adler, D., Ghomashchi, F., Gelb, M. H., Leslie, C. C., Oates, J. A., and Boutaud, O. (2011) Functional Characterization of Mutations in Inherited Human cPLA2 Deficiency. *Biochemistry 50*, 1731−1738.

(4) Capper, E. A., and Marshall, L. A. (2001) Mammalian phospholipases A2: Mediators of inflammation, proliferation and apoptosis. *Prog. Lipid Res. 40*, 1731−1738.
(5) Scott, K. F., Sajinovic, M., Hein, J., Nixdorf, S., Galettis, P., Liauw, W., de Souza, P., Dong, Q., Graham, G. G., and Russell, P. J. (2010) Emerging roles for phospholipase A2 enzymes in cancer. *Biochimie 92*, 601−610.
(6) Granata, F., Staiano, R. I., Loffredo, S., Petraroli, A., Genovese, A., Marone, G., and Triggiani, M. (2010) The role of mast cell-derived secreted phospholipases A2 in respiratory allergy. *Biochimie 92*, 588−593.
(7) Chiricozzi, E., Fernandez-Fernandez, S., Nardicchi, V., Almeida, A., Bolanos, J. P., and Goracci, G. (2010) Group IIA secretory phospholipase A2 (GIIA) mediates apoptotic death during NMDA receptor activation in rat primary cortical neurons. *J. Neurochem. 112*, 1574−1583.
(8) Burke, J. E., Karbarz, M. J., Deems, R. A., Li, S., Woods, V. L., and Dennis, E. A. (2008) Interaction of Group IA Phospholipase A2 with Metal Ions and Phospholipid Vesicles Probed with Deuterium Exchange Mass Spectrometry. *Biochemistry 47* (24), 6451−6459.
(9) Pande, A. H., Qin, S., Nemec, K. N., He, X., and Tatulian, S. A. (2006) Isoform-Specific Membrane Insertion of Secretory Phospholipase A2 and Functional Implications. *Biochemistry 45*, 12436−12447.
(10) Scott, D. L., White, S. P., Browning, J. L., Rosa, J. J., Gelb, M. H., and Sigler, B. P. (1991) Structures of free and inhibited human secretory phospholipase A2 from inflammatory exudate. *Science 254*, 1007−1009.
(11) Diez, E., Louis-Flambergj, P., Hall, R. H., and Mayer, R. J. (1992) Substrate Specificities and Properties of Human Phospholipases A2 in a Mixed Vesicle Model. *J. Biol. Chem. 267*, 18342−18348.
(12) Jain, M. K., Ranadive, G., Yu, B. Z., and Verheij, H. M. (1991) Interfacial Catalysis by Phospholipase A2: Monomeric Enzyme Is Fully Catalytically Active at the Bilayer Interface. *Biochemistry 30*, 7330−7340.
(13) Jain, M. K., Rogers, J., Jahagirdar, D. V., Marecek, J. F., and Ramirez, F. (1986) Kinetics of interfacial catalysis by phospholipase A2 in intravesicle scooting mode, and heterofusion of anionic and zwitterionic vesicles. *Biochim. Biophys. Acta 860*, 435−447.
(14) Jain, M. K., Rogers, J., and DeHaas, G. H. (1988) Kinetics of binding of phospholiphase A2 to lipid/water interfaces and its relationship to interfacial activation. *Biochim. Biophys. Acta 940*, 51−62.
(15) Ray, S., Scott, J. L., and Tatulian, S. A. (2007) Effects of Lipid Phase Transition and Membrane Surface Charge on the Interfacial Activation of Phospholipase A2. *Biochemistry 46*, 13089−13100.
(16) Wacklin, H. P. (2009) Interfacial Mechanism of Phospholipase A2: pH-Dependent Inhibition and Me-β-cyclodextrin Activation. *Biochemistry 48*, 5874−5881.
(17) Connelly, L., Jang, H., Teran Arce, F., Ramachandran, S., Kagan, B. L., Nussinov, R., and Lal, R. (2012) Effects of Point Substitutions on the Structure of Toxic Alzheimer's β-Amyloid Channels: Atomic Force Microscopy and Molecular Dynamics Simulations. *Biochemistry 51*, 3031−3038.
(18) Hung, A., and Yarovsky, I. (2011) Gap Junction Hemichannel Interactions with Zwitterionic Lipid, Anionic Lipid, and Cholesterol: Molecular Simulation Studies. *Biochemistry 50*, 1492−1504.
(19) Norimatsu, Y., Ivetac, A., Alexander, C., Kirkham, J., O'Donnell, N., Dawson, D. C., and Sansom, M. S. P. (2012) Cystic Fibrosis Transmembrane Conductance Regulator: A Molecular Model Defines the Architecture of the Anion Conduction Path and Locates a "Bottleneck" in the Pore. *Biochemistry 51*, 2199−2212.
(20) Beevers, A. J., Nash, A., Salazar-Cancino, M., Scott, D. J., Notman, R., and Dixon, A. M. (2012) Effects of the Oncogenic V664E Mutation on Membrane Insertion, Structure, and Sequence-Dependent Interactions of the Neu Transmembrane Domain in Micelles and Model Membranes: An Integrated Biophysical and Simulation Study. *Biochemistry 51*, 2558−2568.
(21) Allen, W. J., and Bevan, D. R. (2011) Steered Molecular Dynamics Simulations Reveal Important Mechanisms in Reversible Monoamine Oxidase B Inhibition. *Biochemistry 50*, 6441−6454.
(22) Zhou, F., and Schulten, K. (1996) Molecular dynamics study of phospholipase A2 on a membrane surface. *Proteins: Struct., Funct., Genet. 25*, 12−27.
(23) Bond, P. J., Holyoake, J., Ivetac, A., Khalid, S., and Sansom, M. S. P. (2007) Coarse-grained molecular dynamics simulations of membrane proteins and peptides. *J. Struct. Biol. 157*, 593−605.
(24) Bond, P. J., and Sansom, M. S. P. (2006) Insertion and assembly of membrane proteins via simulation. *J. Am. Chem. Soc. 128*, 2697−2704.
(25) Sansom, M. S. P., Scott, K. A., and Bond, P. J. (2008) Coarse-grained simulation: A high-throughput computational approach to membrane proteins. *Biochem. Soc. Trans. 36*, 27−32.
(26) Treptow, W., Marrink, S. J., and Tarek, M. (2008) Gating motions in voltage-gated potassium channels revealed by coarse-grained molecular dynamics simulations. *J. Phys. Chem. B 112*, 3277−3282.
(27) Wee, C. L., Balali-Mood, K., Gavaghan, D., and Sansom, M. S. P. (2008) The Interaction of Phospholipase A2 with a Phospholipid Bilayer: Coarse-Grained Molecular Dynamics Simulations. *Biophys. J. 95*, 1649−1657.
(28) Jain, M. K., Egmond, M. R., Verheij, H. M., Apitz-Castro, R., Dijkman, R., and de Haas, G. H. (1982) Interaction of phospho-lipase A2 and phospholipid bilayers. *Biochim. Biophys. Acta 688*, 341−348.
(29) Marrink, S. J., de Vries, A. H., and Mark, A. E. (2004) Coarse Grained Model for Semiquantitative Lipid Simulations. *J. Phys. Chem. B 108*, 750−760.
(30) Monticelli, L., Kandasamy, S. K., Periole, X., Larson, R. G., Tieleman, D. P., and Marrink, S.-J. (2008) The MARTINI Coarse-Grained force field: Extension to proteins. *J. Chem. Theory Comput. 4*, 819−834.
(31) Marrink, S. J., Risselada, H. J., Yefimov, S., Tieleman, D. P., and de Vries, A. H. (2007) The MARTINI Force Field: Coarse Grained Model for Biomolecular Simulations. *J. Phys. Chem. B 111*, 7812−7824.
(32) Euston, S. R. (2010) Molecular Dynamics Simulation of Protein Adsorption at Fluid Interfaces: A Comparison of All-Atom and Coarse-Grained Models. *Biomacromolecules 11*, 2781−2787.
(33) Atilgan, A. R., Durell, S. R., Jernigan, R. L., Demirel, M. C., Keskin, O., and Bahar, I. (2001) Anisotropy of fluctuation dynamics of proteins with an elastic network model. *Biophys. J. 80*, 505−515.
(34) Tatulian, S. A., Qin, S., Pande, A. H., and He, X. (2005) Positioning membrane proteins by novel protein engineering and biophysical approaches. *J. Mol. Biol. 351*, 939−947.
(35) Berendsen, H. J. C., Postma, J. P. M., van Gunsteren, W. F., DiNola, A., and Haak, J. R. (1984) Molecular dynamics with coupling to an external bath. *J. Chem. Phys. 81*, 3684−3690.
(36) Berendsen, H. J. C. (1991) Transport properties computed by linear response through weak coupling to a bath. In *Computer Simulations in Material Science* (Meyer, M., and Pontikis, V., Eds.) Kluwer, Dordrecht, The Netherlands.
(37) van der Spoel, D., Lindahl, E., Hess, B., Groenhof, G., Mark, A. E., and Berendsen, H. J. (2005) GROMACS: Fast, flexible, and free. *J. Comput. Chem. 26*, 1701−1718.
(38) Bekker, H., Berendsen, H. J. C., Dijkstra, E. J., Achterop, S., van Drunen, R., van derSpoel, D., Sijbers, A., Keegstra, H., Reitsma, B., and Renardus, M. K. R. (1993) Gromacs: A parallel computer for molecular dynamics simulations. In *Physics Computing* (de Groot, R. A., and Nadrchal, J., Eds.) World Scientific, Singapore.
(39) Berendsen, H. J. C., van der Spoel, D., and van Drunen, R. (1995) GROMACS: A message-passing parallel molecular dynamics implementation. *Comput. Phys. Commun. 91*, 43−56.
(40) Lindahl, E., Hess, B., and van der Spoel, D. (2001) Gromacs 3.0: A package for molecular simulation and trajectory analysis. *J. Mol. Model. 7*, 306−317.
(41) MacKerell, A. D., Jr., Bashford, D., Bellott, M., Dunbrack, R. L., Jr., Evanseck, J. D., Field, M. J., Fischer, S., Gao, J., Guo, H., Ha, S., Joseph-McCarthy, D., Kuchnir, L., Kuczera, K., Lau, F. T. K., Mattos, C., Michnick, S., Ngo, T., Nguyen, D. T., Prodhom, B., Reiher, W. E., III, Roux, B., Schlenkrich, M., Smith, J. C., Stote, R., Straub, J., Watanabe, M., Wiorkiewicz-Kuczera, J., Yin, D., and Karplus, M.

(1998) All-atom empirical potential for molecular modeling and dynamics studies of proteins. *J. Phys. Chem. B 102*, 586−3616.
(42) Klauda, J. B., Venable, R. M., Freites, J. A., O'Connor, J. W., Tobias, D. J., Mondragon-Ramirez, C., Vorobyov, I., MacKerell, A. D. J., and Pastor, R. W. (2010) Update of the CHARMM All-Atom Additive Force Field for Lipids: Validation on Six Lipid Types. *J. Phys. Chem. B 114*, 7830−7843.
(43) MacKerell, A. D., Jr., Feig, M., and Brooks, C. L., III (2004) Extending the treatment of backbone energetics in protein force fields: Limitations of gas-phase quantum mechanics in reproducing protein conformational distributions in molecular dynamics simulations. *J. Comput. Chem. 25*, 1400−1415.
(44) Rzepiela, A. J., Schafer, L. V., Goga, N., Risselada, H. J., de Vries, A. H., and Marrink, S.-J. (2009) Reconstruction of Atomistic Details from Coarse-Grained Structures. *J. Comput. Chem. 31*, 1333−1343.
(45) Jorgensen, W. L., Chandrasekhar, J., Madura, J. D., Impey, R. W., and Klein, M. L. (1983) Comparison of simple potential functions for simulating liquid water. *J. Chem. Phys. 79*, 926−935.
(46) Darden, T., York, D., and Pedersen, L. (1993) Particle mesh Ewald: An N-log(N) method for Ewald sums in large systems. *J. Chem. Phys. 98*, 10089−10092.
(47) Essmann, U., Perera, L., Berkowitz, M. L., Darden, T., Lee, H., and Pedersen, L. G. (1995) A smooth particle mesh Ewald potential. *J. Chem. Phys. 103*, 8577−8592.
(48) Hess, B., Bekker, H., Berendsen, H. J. C., and Fraaije, J. G. E. M. (1997) LINCS: A linear constraint solver for molecular simulations. *J. Comput. Chem. 18*, 1463−1472.
(49) Hoover, W. G. (1985) Canonical dynamics: Equilibrium phase-space distributions. *Phys. Rev. A 31*, 1695−1697.
(50) Parrinello, M., and Rahman, A. (1981) Polymorphic transitions in single crystals: A new molecular-dynamics method. *J. Appl. Phys. 52*, 7182−7190.
(51) Jain, M. K., and Vaz, W. L. C. (1987) Dehydration of the lipid-protein microinterface on binding of phospholipase A2 to lipid bilayers. *Biochim. Biophys. Acta 905*, 1−8.
(52) Jain, M. K., and Maliwal, B. P. (1993) Spectroscopic properties of the states of pig pancreatic phospholipase A2 at interfaces and their possible molecular origin. *Biochemistry 32*, 11838−11846.
(53) Kramer, R. M., and Pepinsky, R. B. (1989) Structure and properties of a human non-pancreatic phospholipase A2. *J. Biol. Chem. 264*, 5768−5775.
(54) De Luca, D., Minucci, A., Cogo, P., Capoluongo, E. D., Conti, G., Pietrini, D., Carnielli, V. P., and Piastra, M. (2011) Secretory phospholipase A2 pathway during pediatric acute respiratory distress syndrome: A preliminary study. *Pediatric Critical Care Medicine 12*, 20−24.
(55) Henderson, W. R. J., Oslund, R. C., Bollinger, J. G., Ye, X., Tien, Y. T., Xue, J., and Gelb, M. H. (2011) Blockade of Human Group X Secreted Phospholipase A2 (GX-sPLA2)-induced Airway Inflammation and Hyperresponsiveness in a Mouse Asthma Model by a Selective GX-sPLA2 Inhibitor. *J. Biol. Chem. 286*, 28049−28055.
(56) Huang, C.-h., and Li, S. (1999) Calorimetric and molecular mechanics studies of the thermotropic phase behavior of membrane phospholipids. *Biochim. Biophys. Acta 1422*, 273−307.
(57) Jacob, M., Salesse, C., and Lafleur, M. (1998) Polymorphism of the 1-Palmitoyl-2-arachidonoyl-phosphatidyl-ethanolamine/Dimyristoyl-phosphatidylmethanol Mixture, a Phospholipase A2 Substratem. *Biochem. Biophys. Res. Commun. 251*, 879−882.